The Cryosphere Discuss., https://doi.org/10.5194/tc-2017-208
Manuscript under review for journal The Cryosphere
Discussion started: 14 November 2017

The Cryosphere Discussions
Open Access
EGU

Melting and fragmentation laws from the evolution of two large southern ocean icebergs

Nicolas Bouhier[1], Jean Tournadre[1], Frédérique Rémy[2], and Rozenn Gourves-Cousin[1]

[1]Laboratoire d'Océanographie Physique et Spatiale, IFREMER, Université Bretagne-Loire, Plouzané, France
[2]Laboratoire d'Etudes en Géophysique et Océanographie Spatiales, UMR 5566 | CNES - CNRS , Toulouse, France

Correspondence to: Jean Tournadre
(Jean Tournadre@ifremer.fr)

Abstract. The evolution of the thickness and area of two large southern ocean icebergs, having drifted in open water for more than a year, is estimated through the combined analysis of altimeter data and visible satellite images. Most of the iceberg modelling studies uses two main melting formulations that are compared with the observed thickness evolution of our two icebergs, to test their validity in case of large icebergs. The first formulation, based on a fluid dynamics approach, would tend to underestimate basal melt rates, so that using the second one (using a thermodynamic budget consideration) may be more relevant. Fragmentation is, before melting, the major decay process of large icebergs, yet it is a complex and still poorly documented mechanism. A correlation analysis between the observed volume loss of our two icebergs and environmental parameters highlights those most likely to promote fragmentation. Consequently, a bulk model of fragmentation depending on ocean temperature and iceberg velocity is established and is shown to be able to reproduce well the observed volume variations. Finally, the size distribution of the calved pieces is estimated using both altimeter data and visible images and is found to be consistent with previous studies as typical of brittle fragmentation processes. These results are valuable to account for a more realistic representation of the freshwater flux constrained by large icebergs in models.

1 Introduction

According to recent studies (Silva et al., 2006; Tournadre et al., 2015, 2016), most of the total volume of ice (~60%) calved from the Antarctic continent is transported into the Southern Ocean by large icebergs (i.e. >18km in length). However, their melting accounts for less than 20% of their mass loss, mainly done (80%) through breaking into smaller icebergs (Tournadre et al., 2016). Large icebergs actually act as a buffer to transport ice away from the Antarctic Coastline into the ocean interior while fragmentation can be viewed as a diffuse process. It generates plumes of small icebergs that melt far more efficiently than larger ones and whose geographical distribution constrains the freshwater input into the ocean.

Global ocean models including iceberg components (Gladstone et al., 2001; Jongma et al., 2009; Martin and Adcroft, 2010; Marsh et al., 2015; Merino et al., 2016) show very different effects between basal ice-shelf and iceberg melting. Numerical model runs with and without icebergs show that the inclusion of icebergs in a fully coupled general circulation model (GCM) results in significant changes in the modelled ocean circulation and sea-ice conditions around Antarctica (Jongma et al., 2009; Martin and Adcroft, 2010; Merino et al., 2016). The transport of ice away from the coast by icebergs and the associated

The Cryosphere Discuss., https://doi.org/10.5194/tc-2017-208
Manuscript under review for journal The Cryosphere
Discussion started: 14 November 2017

freshwater flux cause these changes (Jongma et al., 2009). Although the results of these modelling studies are not always in agreement in terms of ocean circulation or sea ice extent they all highlight the important role that icebergs play in the climate system, and they also show that models that do not include an iceberg component are effectively introducing systematic biases (Martin and Adcroft, 2010).

However, despite these modelling efforts, the current generation of iceberg models are not yet able to represent the full range of iceberg sizes observed in nature from growlers ($\leq$ 10 m) to "giant" tabular icebergs ($\geq$ 10 km).

The iceberg size distribution has also strong impact on both circulation and sea ice as shown by Stern et al. (2016). Furthermore, all current iceberg models fail in accounting for the size transfer of ice induced by fragmentation, as in these models small icebergs can't stem from the breaking of bigger ones.

The two main decay processes of icebergs, melting and fragmentation, are still quite poorly documented and not fully represented in numerical models. Although iceberg melting has been widely studied (Huppert and Josberger, 1980; Neshyba, 1980; Hamley and Budd, 1986; Jansen et al., 2007; Jacka and Giles, 2007; Helly et al., 2011), very few validations of melting law have been published (Jansen et al., 2007), especially for large icebergs. Large uncertainties still remain on the melting laws to be used in numerical models.

The calving of icebergs from glaciers and ice shelves has been quite well studied (e.g (Holdsworth and Glynn, 1978; Fricker et al., 2002; Benn et al., 2007; MacAyeal et al., 2006; Amundson and Truffer, 2010)) and empirical calving laws have been proposed (Amundson and Truffer, 2010; Bassis, 2011). However, very few studies have been dedicated to the breaking of icebergs. (Savage, 2001) analysing Greenland icebergs decay proposed three distinct fragmentation mechanisms. Firstly, flexural breakups by swell induced vibrations in the frequency range of the iceberg bobbing on water that could cause fatigue and fracture at weak spots (Goodman et al., 1980; Schwerdtfeger, 1980; Wadhams et al., 1983). Secondly, two mechanisms resulting from wave erosion at the waterline, calving of ice overhangs and buoyant footloose mechanism (Wagner et al., 2014). (Scambos et al., 2008), using satellite images, ICESat altimeter and field measurements analysed the evolution of two Antarctic icebergs and identified three styles of calving during the drift : "rift calving" that corresponds to the calving of large daughter icebergs by fracturing along preexisting flaws, "edge wasting" is the calving of numerous small edge-parallel, sliver shape small icebergs and "rapid disintegration" characterised by the rapid calving of numerous icebergs.

The pieces calved from icebergs drift away from their parent under the action of wind and ocean currents as a function of size, shape and draft (Savage, 2001). These dispersion can create large plumes of icebergs that can represent a significant contribution to the freshwater flux over vast oceanic regions where no large icebergs are observed (Tournadre et al., 2016). The size distribution of the calved pieces is essential to analyse and understand the transfer of ice between the different iceberg scales and thus to estimate the freshwater flux. It is also important for modelling purposes. (Savage et al., 2000) using aerial images and in situ measurements estimated the size distribution of small bergy bits (<20m in length) calved from deteriorating Greenland icebergs. But at present no study has been published on the size distribution of icebergs calved from large Southern Ocean icebergs.

Recent progress in satellite altimeter data analysis allow to estimate the small (<3km in length) iceberg distribution and volume as well as the free-board elevation profile and volume of large icebergs (Tournadre et al., 2016). A database of small

The Cryosphere Discuss., https://doi.org/10.5194/tc-2017-208
Manuscript under review for journal The Cryosphere
Discussion started: 14 November 2017

iceberg location, area and volume from 1992 to present is distributed by CERSAT as well as monthly fields of probability of presence, mean area and volume of ice (Tournadre et al., 2016). It is thus now possible to estimate the thickness variation and thus the melting of large icebergs. A crude estimate of the large iceberg area is also available from the National Ice Center but it is not precise enough to analyse the area loss by fragmentation. A more precise area analysis can be conducted by analysing satellite images such as the Moderate Resolution Imaging Spectro- radiometer (MODIS) ones on the Aqua and Terra satellites (Scambos et al., 2005).

Two large icebergs, B17a and C19a, that drifted for more than one year in open water (see figure 1) away from other large icebergs and that have been very well sampled by altimeters and MODIS have been selected to study the melting and fragmentation of large southern ocean tabular icebergs. Their free-board evolution, and thus thickness, is estimated from satellite altimeter data while their area/size/shape has been estimated from the analysis of MODIS images. Their area and thickness evolution is then used to test the validity of the melting models used in iceberg numerical modelling and to analyse the fragmentation process. The two icebergs were also chosen because they have very different characteristics. While C19a was one of the largest iceberg on record (>1000 km^2) that drifted for more than 2 years in the South Pacific, B17a was a relatively small 200 km^2 one drifting in the Weddell Sea. The large plumes of small icebergs generated by the decay of both icebergs can be detected by altimeters and MODIS images. The ALTIBERG database and selected MODIS images can be used to analysed the size distribution of fragments.

The present paper is organised as follows. The first section describes the data used in the study, including the environmental parameters (such as ocean temperature, current speed, ..) necessary to estimate melting and fragmentation. The second section presents the evolution of the two selected icebergs. In a third section, the two melting laws widely used in the literature, forced convection and thermal turbulence exchange are confronted to the observed melting of B17a and C19a. The following section analyses the fragmentation process and proposes a fragmentation law. It also investigates the size distribution of the pieces calved from the large ones.

2 Data

2.1 Iceberg Data

The National Ice Center (NIC) Southern Hemisphere Iceberg database contains the position and size (length and width) estimated by analysis of visible or SAR images of icebergs larger than 10 nautical miles (19 km) along at least one axis. It is updated weekly. Every iceberg is tracked, and when imagery is available, information is updated and posted. The Brigham Young University Center for Remote Sensing (BYU) Center for Remote Sensing maintains an Antarctic Iceberg Tracking Database for icebergs larger than 6 km in length (Stuart and Long, 2011). Using six different satellite scatterometer instruments, they produced an iceberg tracking database that includes icebergs identified in enhanced resolution scatterometer backscatter. The initial position for each iceberg is located based on a position reported by the NIC or by the sighting of a moving iceberg in a time series of scatterometer images.

The Cryosphere Discuss., https://doi.org/10.5194/tc-2017-208
Manuscript under review for journal The Cryosphere
Discussion started: 14 November 2017

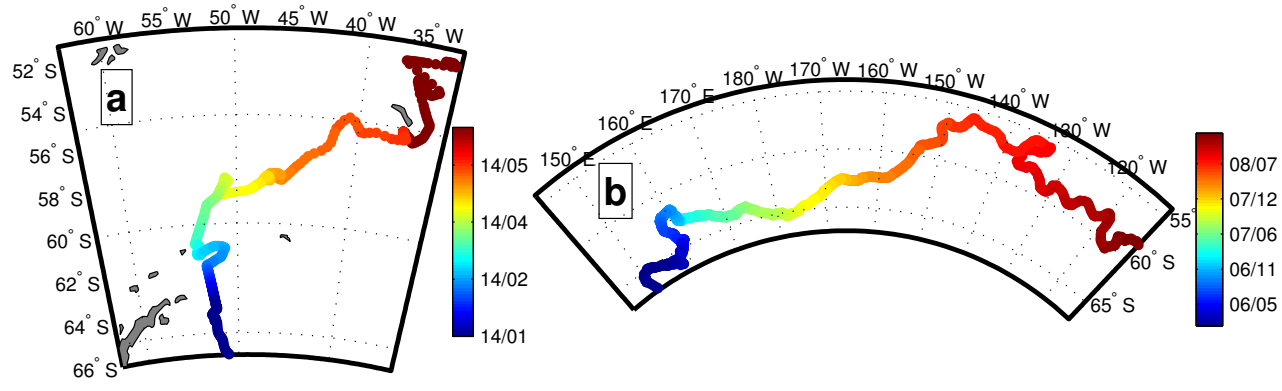

Figure 1. Trajectories of B17a (a) and C19a (b) icebergs. The colorscale represents the time along the trajectory.

In 2007, Tournadre (2007) demonstrated that any target emerging from the sea surface (such as iceberg) can produce a detectable signature in HR altimeter wave forms. Their method enables to detect icebergs in open ocean only, and to estimate their area. Due to constrains on the method, only icebergs between 0.1km^2 and ~9 km^2 can be detected. Nine satellite altimetry missions have been processed to produce a 1992-present database of small icebergs location (latitude, longitude), area, volume and mean backscatter (Tournadre et al., 2016). The monthly mean probability of presence, area and volume of ice over a regular polar (100x100 km^2) or geographical (1^ox2^o) grid are also available and are distributed on the CERSAT website.

Altimeters can also be used to measure the free-board elevation profile of large icebergs (McIntyre and Cudlip, 1987; Tournadre et al., 2015). Combining iceberg tracks from NIC and the archives of three Ku band altimeters, Jason-1, Jason-2 and Envisat, Tournadre et al. (2015) created a database of daily position, free-board profile, length, width, area and volume of all the NIC/BYU large icebergs covering the 2002-2012 period. For example, B17a was sampled by 152 altimeter passes during its drift and C19a by 258 ones (see figure 2).

2.2 Visible Images

The weekly estimates of iceberg lengths and widths provided by NIC are manually estimated from satellite images and they are not accurate enough to precisely compute the iceberg area and its evolution. A careful re-analysis of the MODIS imagery from the Aqua and Terra satellites was thus conducted to precisely estimate the C19a and B17a area until their final collapse. The images have been systematically collocated with the two icebergs using the NIC/BUY track data. It should be noted that in some areas of high iceberg concentration, especially when B17a reaches the “iceberg alley”, NIC/BYU regularly mistakenly

The Cryosphere Discuss., https://doi.org/10.5194/tc-2017-208
Manuscript under review for journal The Cryosphere
Discussion started: 14 November 2017

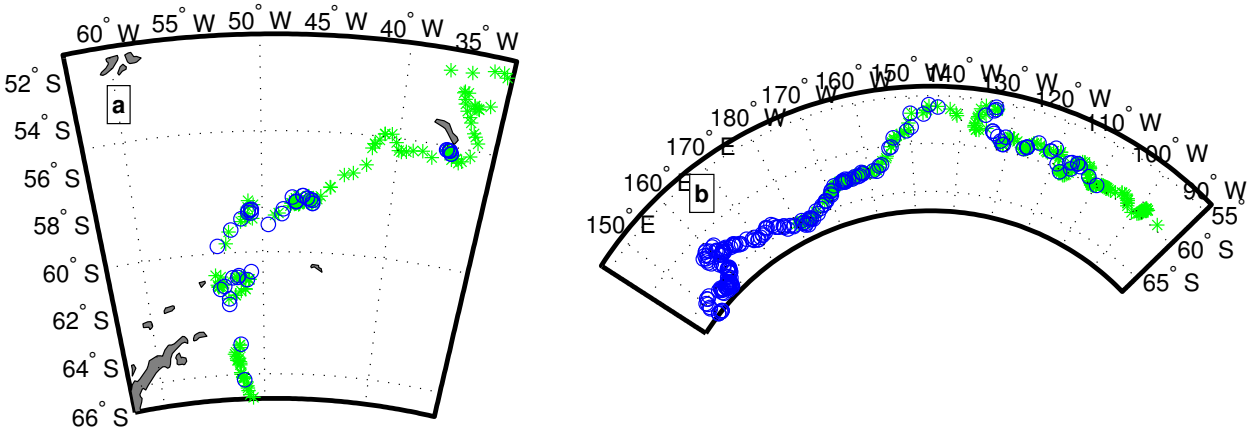

Figure 2. Sampling of B17a (a) and C19a (b) icebergs by MODIS (green stars) and altimeters (blue circles).

followed another iceberg, or lost its track when it became quite small. More than 1500 images were collocated and selected. The level 1B calibrated radiances from the two higher resolution (250 m) channels (visible channels 1 and 2 at 645 and 860 nm frequencies) were used to estimate the iceberg's characteristics. For each image whose cloud clover and light conditions were good, a supervised shape analysis was performed. Firstly, a threshold depending on the image light conditions is estimated and used to compute a binary image. The connected components of the binary image are then determined using standard Matlab© image processing tools and finally the iceberg's properties, centroid position, major and minor axis lengths and area are estimated. On a number of occasions the iceberg's surface was obscured by clouds but visual estimation was possible because the image contrast was sufficient to discern edges through clouds. For these instances the iceberg's edge and shape were manually estimated. The final analysis is based on 286 valid images for B17a, and 503 for C19a. The locations of the MODIS images for B17a and C19a are given in figure 2 while four examples of iceberg area estimates are given in figure 3. The comparison of area for consecutive images shows that the area precision is around 2-3%.

2.3 Ancillary data

Several environmental parameters along the icebergs trajectories are also used in this study. Due to the lack of a better alternative, the sea surface temperature (SST) is used as a proxy of the water temperature. The level-4 satellite analysis product ODYSSEA, distributed by the Group for High-Resolution Sea Surface Temperature (GHRSST) has been used. It is generated by merging infrared and microwave sensors and using optimal interpolation to produce daily cloud-free SST fields at a 10 km resolution over the globe. The sea ice concentration data are from the CERSAT level-3 daily concentration product, available on a 12.5 km polar stereographic grid from the SSM/I radiometer observations. The wave height and wave peak frequencies come from the global Wave Watch3 hindcast products from the IOWAGA project (http://wwz.ifremer.fr/iowaga/). The AVISO

The Cryosphere Discuss., https://doi.org/10.5194/tc-2017-208
Manuscript under review for journal The Cryosphere
Discussion started: 14 November 2017

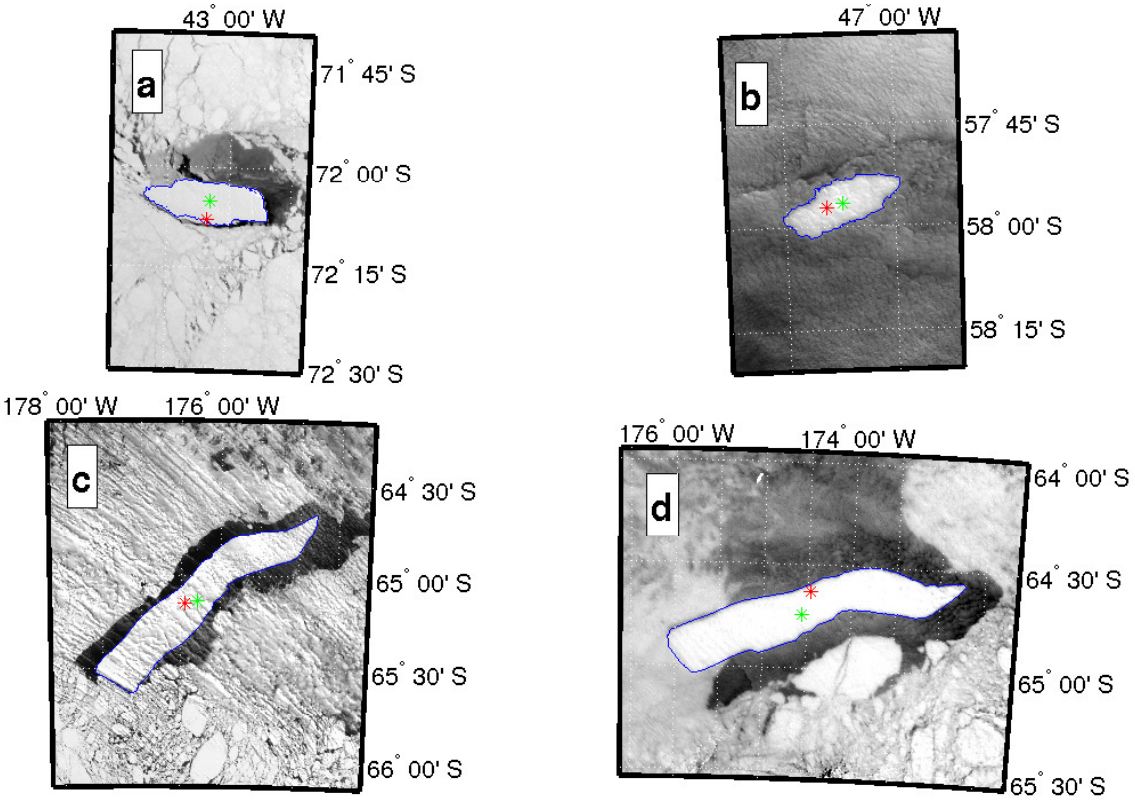

Figure 3. Example of B17a (a and b) and C19a (c and d) area estimate using Modis images. The blue lines represent the iceberg perimeter, the red and green crosses represent the NIC and MODIS iceberg's positions respectively.

Maps of Absolute Dynamic Topography & absolute geostrophic velocities (MADT) provides a daily multi-mission absolute geostrophic current on a 0.25 ° regular grid that is used to estimate the current velocities at the iceberg locations.

3 Melting and fragmentation of B17a and C19a

3.1 B17a

Iceberg B17a originates from the breaking of giant tabular B17 near Cape Hudson in 2002. It then drifted for 10 years along the continental slope within the "coastal current", until it reached the Weddell Sea in summer 2012 (see figure 1-a). It travelled within sea ice at a speed ranging from 2 to 12 cm.s^{-1}, coherent with previous observational studies (Schodlok et al., 2006). It crossed the Weddell Sea while drifting within sea ice and reached open water in April 2014. It was then caught in the western branch of the Weddell gyre and drifted north in the Scotia Sea until it grounded, in October 2014, near South Georgia, a common

The Cryosphere Discuss., https://doi.org/10.5194/tc-2017-208
Manuscript under review for journal The Cryosphere
Discussion started: 14 November 2017

grounding spot for icebergs. It remained there for almost 6 months until it finally left its trap in March 2015 and drifted back northward until it final demise in early June 2015. B17a was a "medium size" big iceberg, with primary dimensions of 35 x 14 km^2 and an estimated free-board of 52 m, resulting in an original volume of 113 km^3 and a corresponding mass of ~103 Gt. Before 2014, B17a free-board and area remained almost constant while it drifted within sea ice. After March 2014, B17a started to drift in open water and to melt and break. During its drift in open water, from March 2014 to June 2015, B17a was sampled by 200 MODIS images and 41 altimeter passes. Figure 4-a presents the satellite free-board and area measurements as well as the daily interpolated values. During this drift in the Weddell Sea, it experienced different basal melting regimes : firstly, while it left the peninsula slope current, with negative SST's and low drift speeds (see figure 4-b and -d), it was subject to an average melt rate of 5.7m.month^{-1}; then it drifted more rapidly within the Scotia Sea and experienced a mean thickness decrease of 15 m.month^{-1}, and finally it melted at a rate close to 20m.month^{-1} as it accelerated its drift before its grounding. As for fragmentation, the area loss is limited (40 km^2 in 250 days, i.e. less than 10%) but then accelerates as B17a got trapped (80 km^2 in 70 days). The area loss slows down for the second half of the grounding, only to increase dramatically as B17a is released and collapses a few days later. This could be related to an embrittlement of the iceberg structure, potentially under the action of unbalanced buoyancy forces while grounded (Venkatesh, 1986; Wagner et al., 2014).

The total volume loss, basal melting, breaking are presented in figure 4-e. These terms are computed from the mean thickness and area as follow: the basal melting volume loss M is the sum of the products of iceberg surface, S, by the daily variation of thickness, dT

$$M(i) = S(i)dT(i) \tag{1}$$

and the breaking loss B is the sum of the products of thickness, T, by the daily variation of surface, dS

$$B(i) = dS(i)T(i) \tag{2}$$

As B17a started to drift in open water its mass varied first slowly mainly through melting. Between January 2014 and March 2015, basal melting accounts for more than 60 % of the total volume loss, whereas fragmentation is responsible for 30% of the loss. However, after November 2014 breaking becomes preponderant as the icebergs started to break up more rapidly.

3.2 C19a

Our second iceberg of interest is the giant C19a which is one of the fragments resulting from the splitting of C19, the second largest tabular iceberg on record. C19a was born offshore Cap Adare (170°E) in 2003 and was originally oblong and narrow, around 165 km long and 32 km wide with an estimated free-board of ~40 m, i.e. a volume of about 1000 km^3 and a mass of 900 Gt. It drifted mainly north eastward for almost 4 years, in sea ice for most of the time, until it first entered open ocean in summer 2005 (see figure 1). It was temporarily re-trapped by the floes in winter 2006 and eventually left the ice coverage permanently in late spring 2007. It drifted then within the Antarctic circumpolar current and eventually close to the polar front and its warm

The Cryosphere Discuss., https://doi.org/10.5194/tc-2017-208
Manuscript under review for journal The Cryosphere
Discussion started: 14 November 2017

waters until its final demise in April 2009 in the Bellingshausen Sea. Before November 2007, C19a experienced very little change except a very mild melting (not presented in the figure). Its volume was 880 km^3 (~790 Gt) in December 2007 when it entered definitively the open sea. During its final drift, from December 2007 to March 2009, C19a was sampled by 317 MODIS images and 69 altimeter passes (see figure 2). The C19a area and free-board are presented in figure 5 as well as SST, sea state and volume loss.While the volume loss was mainly due to melting before this date, breaking dominated afterwards. Basal melting only explains 25% of the total volume decrease (see figure 5-e). It is to be noted that B17 thickness loss was almost 5 times faster than that of C19, the latter experiencing mean basal melt rates ranging from 1 m.month^{-1} to 3 m.month^{-1} in most of its drift (and as much as 13 m.month^{-1}in its last month, characterised by very high water temperatures). As for fragmentation, its main volume loss mechanism (75%), its area loss was first mild while it progressed in colder waters (around 2.6 km^2.day^{-1}), and starts to increase as soon as it enters in positive temperature waters with an average loss of 9.5 km^2.day^{-1} and with dramatic shrinkage of 340 km² and 370 km² lost in 10 days that corresponds to large fragmentation events.

4 Melting models

Apart from fragmentation, the basal melting of iceberg accounts for the largest part of the total mass loss Martin and Adcroft (2010), Tournadre et al. (2015). Although firn densification (see Appendix) and surface melting can also contribute, it is the main cause of thickness decrease. It can be mainly attributed to the turbulent heat transfer arising from the difference of speed between the iceberg and surrounding water. Two main approaches have been used to compute the melting rate and to model the evolution of iceberg and the freshwater flux (see for example Bigg et al. (1997); Gladstone et al. (2001); Silva et al. (2006); Jongma et al. (2009); Merino et al. (2016); Jansen et al. (2007)). The first one is based on the forced convection formulation proposed by (Weeks and Campbell, 1973), while the second one uses the thermodynamic formulation of (Hellmer and Olbers, 1989) and the turbulent exchange velocity at the ice-ocean boundary. The B17a and C19a data sets allow to confront these two formulations with melting measurements for two icebergs of different shapes and sizes and under different environmental conditions and to test their validity for large icebergs.

4.1 Forced convection of Weeks and Campbell

The forced convection approach of Weeks and Campbell (1973) is based on the fluid mechanics formulation of heat-transfer coefficient for a fully turbulent flow of fluid over a flat plate. The basal convective melt rate M_b is a function of both temperature and velocity differences between the iceberg and the ocean. It is expressed (in m.day^{-1}) as (Gladstone et al., 2001; Bigg et al., 1997):

$$M_b = 0.58|\overrightarrow{V_w} - \overrightarrow{V_i}|^{0.8}\frac{T_w - T_i}{L^{0.2}} \tag{3}$$

with $\overrightarrow{V_w}$ being the current speed (at the base of the iceberg), $\overrightarrow{V_i}$ the iceberg speed, T_i and T_w the iceberg and water temperature and L the iceberg's length (longer axis). This expression has been widely used in numerical models (Bigg et al., 1997; Gladstone et al., 2001; Martin and Adcroft, 2010; Merino et al., 2016; Wagner et al., 2017). As water temperature at keel depth is not

The Cryosphere Discuss., https://doi.org/10.5194/tc-2017-208
Manuscript under review for journal The Cryosphere
Discussion started: 14 November 2017

available, the sea surface temperature (SST) is used as a proxy. The SST for each iceberg is presented in figures 4 and 5. The first unknown quantity in (3), the iceberg's temperature T_i can be at the time of calving as low as -20°C (Diemand, 2001). After a stay in water for sometimes several years, the iceberg's surface temperature will depend on the ablation rate. When ablation is limited, i.e. in cold waters, the ice can warm up theoretically up to 0°C, while in warmer waters the rapid disappearance of the outer layers tends to leave colder ice near the surface. The surface ice temperature could thus theoretically vary from -20°C to 0°C but is commonly taken at -4°C (Løset, 1993; Martin and Adcroft, 2010; Gladstone et al., 2001).

The mean daily iceberg speed can be easily estimated from the iceberg track. Numerical ocean circulation model are not precise enough to provide realistic current speed in this region. The comparison of iceberg velocities and AVISO geostrophic currents presented in Figures 4 and 5 shows that the iceberg velocity is sometimes significantly larger than the AVISO ones. They are thus not reliable enough to compute the melt rate. V_w is thus considered as unknown.

The basal melt is computed using Equation 3 for V_w from 0 to 3 m.s^{-1} by 0.01 steps and T_i from -20 to 2°C by 0.1°C steps. The positive temperatures are used to test the model's convergence.

The uncertainties on the different parameters and measurements are too large for a direct comparison of the modelled and measured daily melt rate. However, it is possible to to test the model validity by comparing the bulk melting rate, i.e. the modelled and measured cumulative loss of thickness, $\Sigma_{i=1}^{n} M_b(t_i)$.

As current velocities and iceberg temperature are not constant during the iceberg's drift, the modelled thickness loss is fitted by linear regression to the measured one for each time step t_i over a $\pm$20-day period to estimate $V_w(t_i)$ and $T_i(t_i)$.

When no SST is available, i.e. when the iceberg is within sea ice for a short period, T_w is fixed to the sea water freezing temperature.

The model allows to reproduce extremely well the thickness variations with correlation larger than 99.9% for both B17a and C19a (see figures 6-a and 7-a) and mean differences of thickness loss of 3.1 and 0.5 m respectively and maximum differences less than 8 and 1.5 m. However, the current velocity inferred from the model, presented in Figures 6-b and 7-b, reaches very high and unrealistic values (> 2 m.s^{-1}). Compared to the altimeter geostrophic currents from AVISO the current speed can be overestimated by more than a factor of 10.

The second model parameter T_i (see Figures 6-c and 7-c) varies between -20°C and -0.6°C with a -10.9 ± 7.1°C mean for B17a and -9°C and 1°C with a -10.6 ± 5.8 °C mean for C19a. For C19a, the model sometimes fails to converge to realistic iceberg temperature, i.e. for $T_i < 0$°C. It happens when the measured melting is weak and SST are positive (for example from January to May 2007, figures 7-c and 5-b). The model can reproduce this inhibition by taking down the water/ice temperature difference to zero resulting in an artificial increase of the iceberg temperature to positive values . For B17a, the model always converges and the lower temperatures (-20°C) are observed during extremely rapid melting period or during the grounding period. It could reflect the decrease of ice surface temperature during rapid ablation events or an underestimation of the melt rate.

The large overestimation of current speed indicates that the model tends to generally underestimate the melting rate and that unrealistically high speeds are necessary to reproduce the observed melting. It also fail to reproduce weak melting events that sometimes occurs in positive temperature water. Thus, although the model can reproduce the thickness variations with a high

The Cryosphere Discuss., https://doi.org/10.5194/tc-2017-208
Manuscript under review for journal The Cryosphere
Discussion started: 14 November 2017

precision, the fitting parameters take values that are too high. If realistic values of current speed and iceberg temperature were used, the melt rate would be largely underestimated.

4.2 Thermal turbulent exchange of Hellmer and Olbers

The second melt rate formulation is based on thermodynamic and on heat and mass conservation equations. It assumes heat balance at the iceberg-water interface and was originally formulated for estimating ice-shelves melting (Hellmer and Olbers, 1989; Holland and Jenkins, 1999). The turbulent heat exchange is thus consumed by melting and the conductive heat flow through the ice:

$$\rho_w C_{pw} \gamma_T (T_b - T_w) = \rho_i L M_b - \rho_i C_{pi} \Delta T \; M_b \tag{4}$$

Thus,

$$M_b = \frac{\rho_w C_w \gamma_T}{\rho_i} \frac{T_b - T_w}{L_H - C_{pi} \Delta T} \tag{5}$$

where M_b is the met rate (in m/s^{-1}), $L_H = 3.34.10^5$ J.kg^{-1} is the fusion latent heat, $C_{pw} = 4180$ J.kg^{-1}.K^{-1} and $C_{pi} = 2000$ J.kg^{-1}.K^{-1} are the heat capacity of seawater and ice, respectively. $T_b = -0.0057 S_w + 0.0939 - 7.64.10^{-4} P_w$ is the freezing temperature at the base of the iceberg, S_w and P_w are the salinity and pressure, $\Delta T = T_i - T_b$ represents the temperature gradient within the ice at the iceberg base (Jansen et al., 2007). γ_T is the thermal turbulent velocity that can be expressed as (Kader and Yaglom, 1972)

$$\gamma_T = \frac{u^*}{2.12 \log(u^* l \nu^{-1}) + 12.5 Pr^{2/3} - 9} \tag{6}$$

where $P_r = 13.1$ is the molecular Prandtl number of sea water, $l = 1$ m the mixing length scale, $\nu = 1.83.10^{-6}$ is the water viscosity, and u^* the friction velocity. The latter, which is defined in terms of the shear stress at the ice-ocean boundary, depends on a dimensionless drag coefficient, or momentum exchange coefficient, $C_D = 0.0015$ and the current velocity in the boundary layer, $u \simeq V_w - V_i$, by $u^{*2} = C_D u^2$.

Jansen et al. (2007) modelled the evolution of a large iceberg (A38b) using this formulation for melting. They calibrated their model using IceSat elevation measurements and found γ_T ranging from 0.4 10^{-4}m.s^{-1} to 1.8 10^{-4}m.s^{-1} close to the 1 10^{-4}m.s^{-1} proposed by Holland and Jenkins (1999). Silva et al. (2006) who estimated the Southern Ocean freshwater flux by combining the NIC iceberg data base and a model of iceberg thermodynamics also based on this formulation considered a unique and much larger γ_T of 6. 10^{-4}m.s^{-1} .

The basal melt is thus computed using Equation 5 for γ_T from 0.1 10^{-5} to 10 10^{-4} m.s^{-1} by 0.1 10^{-5} steps and T_i from -20 to 2°C by 0.1°C steps. As for forced convection, the model is fitted for each time step over a ±20 day period to estimate $\gamma_T(t_i)$ and $T_i(t_i)$. The current speed is then estimated using Equation 6.

The Cryosphere Discuss., https://doi.org/10.5194/tc-2017-208
Manuscript under review for journal The Cryosphere
Discussion started: 14 November 2017

This model also reproduces extremely well the thickness variations with correlation better than 99.9% for both B17a and C19a (see Figures 6-b 7-a). The mean differences of thickness is 3.7 and 0.3 m for B17a and C19a respectively and the maximum difference is 14.1 and 0.8 m. The modelled current velocity (Figures 6-b and 7-b) is always smaller than the forced convection one except for B17a during the three months (September to November 2014) of very rapid drift and melting. Although it is still significantly larger than the AVISO one, especially for B17a, the values are more compatible with the ocean dynamics in the region (Jansen et al., 2007).

For B17a, γ_T varies from 0.41 10^{-4} to 10 10^{-4} m.s^{-1} with a (2.9 ± 2.8) 10^{-4}m.s^{-1} mean. If the period of very rapid melting (September to November 2014), during which γ_T increases up to 10.10^{-4}, is not considered, γ_T varies only up to $2.5\ 10^{-4}$m.s^{-1} with a $(1.6 \pm 0.92)10^{-4}$m.s^{-1} mean. These values are comparable to those presented by (Jansen et al., 2007) for A38b whose size was similar to that of B17a. For C19a, γ_T has significantly lower values ranging from $0.3\ 10^{-5}$ to $1.6\ 10^{-4}$m.s^{-1} with $(0.34 \pm 0.37)\ 10^{-4}$m.s^{-1}mean. These values, which correspond to the lower ones found by Jansen et al. (2007), might reflect a different turbulent behaviour for very large iceberg that can modify more significantly their environment especially the ocean circulation (Stern et al., 2016).

The mean iceberg's temperature is -10.8 ± 5.0°C for B17a and -10.6 ± 5.8°C for C19a. It oscillates quite rapidly and certainly more erratically than in reality. Although the current velocity can reach quite high values, this melt reate formulation appears better suited to reproduce the bulk melting of icebergs than forced convection.

5 Fragmentation

As said earlier, fragmentation is the least known and documented decay mechanism of icebergs. It has been suggested that swell induced vibrations in the frequency range of the iceberg bobbing on water could cause fatigue and fracture at weak spots (Wadhams et al., 1983; Goodman et al., 1980). Small initial cracks within the iceberg are likely to propagate in each oscillation until they become unstable resulting in the iceberg fracture (Goodman et al., 1980). Jansen et al. (2005) suggested from model simulations that increasing ocean temperatures along the iceberg drift and enhanced melting cause a rapid ablation of the warmer basal ice layers while the iceberg core cold temperature remains relatively constant and cold. The resulting large temperature gradients at the boundaries could be important for possible fracture mechanics during the final decay of iceberg.

5.1 fragmentation law

Like the calving of iceberg from glacier or ice shelves (Bassis, 2011), fragmentation is a stochastic process that makes individual events impossible to forecast. However, the probability an iceberg will calve during a given interval of time can be described by a probability distribution. This probability distribution depends on environmental conditions that can stimulate or inhibit the fracturing mechanism (MacAyeal et al., 2006). If the environmental parameters conditioning the probability of fracture can be determined, it would thus be possible to propose at least bulk fracturing laws that could be used in numerical models. The correlation between the relative volume loss (i.e. the a-dimensional loss), dV/V, filtered using a 20 day Gaussian window and different environmental parameters : SST, current speed, difference of iceberg and current velocities, wave height, wave peak

The Cryosphere Discuss., https://doi.org/10.5194/tc-2017-208
Manuscript under review for journal The Cryosphere
Discussion started: 14 November 2017

frequency, wave energy at the bobbing period; has thus been analysed in detail. The highest correlation is obtained for SST, with similar values for both icebergs, namely 63% for B17a and 64% for C19a. It is high enough to be statistically significant and to show that SST is certainly one of the main drivers of the fracturing process. SST is followed by the iceberg velocity which has a mild correlation of 30% for B17a and 28% for C19a showing a potential second order impact. The correlation for all the other parameters, in particular for the sea state parameters, is below 15%. Figure 8, which presents the 20 day-Gaussian filtered relative surface loss as function of SST, iceberg velocity and wave height confirms the strong impact of the temperature. The logarithm of the loss clearly increases almost linearly with temperature. The regression gives similar slopes of 1.06±0.04 for B17a and 0.8±0.04 for C19a. There also exist a slight increase of loss with iceberg velocity. The regression slopes are however very different for B17a (1.8±0.8) and C19a (6.3±0.8). The significant wave height has no impact on the loss.

The cumulative sum of the a-dimensional loss for the two icebergs presented in figure 9 exhibit very similar behaviour suggesting that a general fracturing law might exist.

We have decided to investigate this matter by step, by progressively including the dependence to environmental parameters in a simple model of bulk volume loss depending. Firstly, only on the temperature difference between the ocean and the iceberg is considered in the model

$$M_{fr} = \alpha \exp(\beta(T_w - T_i)) \tag{7}$$

where M_{fr} is the relative volume loss by fragmentation and α, β are model coefficients. In a first step the daily volume loss is computed for and compared to the observed ones The model best fit presented in figure 9 (black line) gives similar results for B17a and C19a: $\alpha = 1.9\,10^{-5}$ and $2.7\,10^{-5}$, β= 1.3 and 0.91, T_i = -3.4 and -3.7 ^{o}C respectively. Although the correlation between model and measurement is high (96% and 98% respectively), the model does not reproduce very well the final iceberg's decay.

A possible second order contribution of the iceberg velocity is thus taken into account by introducing a second term in the model in the form:

$$M_{fr} = \alpha \exp(\beta(T_w - T_i))(1 + \exp(\gamma V_i)) \tag{8}$$

The model is first fitted by setting the β coefficient to the value found using the simple model. The best fit of the model is presented as a blue line in figure 9. The fitting parameters have quite similar values for the two icebergs, $\alpha = 5\,10^{-6}$ for both, γ= 5.3 and 6.2 and T_i = -3.3 and -4 ^{o}C respectively. The inclusion of velocity clearly improves the modelling of the final decay and increases the correlation to more than 99.5%.

The possibility of a general law has been further investigated by testing the model with a common β of 1 for both icebergs. The best fit is presented as green lines. The best fit is only slightly degraded (correlation about 99.2%). The γ and T_i fitting parameters slightly vary and are of the same order of magnitude for the two icebergs. Only the α parameter strongly differs for B17a ($3\,10^{-5}$) and C19a ($5\,10^{-6}$). This can result from the fact that the variability of iceberg temperature is not taken into account. Indeed, a change of T_i of ΔT introduces a change of α of $\exp(-\beta \Delta T)$.

The Cryosphere Discuss., https://doi.org/10.5194/tc-2017-208
Manuscript under review for journal The Cryosphere
Discussion started: 14 November 2017

A final model is tested in the same way as the melting law. The α, β and γ parameters are fixed at $1\,10^{-6}$, 1 and 6.5 respectively and the model is fitted at each time step over a $\pm$20 day period to determine the best fit T_i. The model fit the data with correlation higher than 99.8%. The iceberg temperature varies by less than 2^{o}C and has a mean of -3.7 ± 0.6^oC for B17a and -2.9 ± 0.6^oC for C19a (see figure 10).

Other model formulations including wave height, iceberg speed and wave energy at the bobbing period were tested but didn't bring any improvement.

5.2 Transfer of volume and distribution of sizes of fragments

The fragmentation of both icebergs generates large plumes of smaller icebergs that drift on their own path and disperse the ice over large regions of the ocean. The knowledge of the size distribution of the calved pieces is as important as the fragmentation law for modelling purposes as the fragments size will condition their drift and melting and ultimately the freshwater flux. The fragment size distribution is analysed using both the ALTIBERG small icebergs iceberg database and the analysis of three clear MODIS images that present large plumes of pieces calved from C19a and B17a. Figures 11-a and c present the small icebergs detected by altimeters in the vicinity (same day and 400 km in space) of B17a and C19a. To restrict as much as possible a potential influence of icebergs not calved from the one considered, the analysis of the iceberg size is restricted to the period when C19a drifted thousand of kilometres away from any large iceberg. During this period more than 2400 icebergs were detected. The corresponding size distribution is presented in figure 13.

The small iceberg detection algorithm used to analyse the MODIS images is similar to those used to estimate the large iceberg area. Firstly, the cloudy pixels are eliminated by using the difference between channel 1 and 2 radiances. The image is then binarised using a radiance threshold. A shape analysis is then applied to the binary images to detect and characterise the icebergs. The results are then manually validated. Figure 12 presents an example of such a detection for C19a. The full resolution images are available in the Supplementary Information (Figures S1 to S4). The analysis detected 1057, 817, 1228 and 337 icebergs for the four images respectively. The size distributions for the four images and for the overall mean are given also in figure 13. The six distributions are remarkably similar between 0.1 and 5 km^2. The tail of the distributions (i.e. for area larger than 7 km^2) is not statistically significant because too few icebergs larger than 5-6 km^2 were detected.

The slopes of the distributions have thus been estimated by linear regression for areas between 0.1 and 5km^2. The values for the four images are -1.49$\pm$0.13, 1.63$\pm$0.15, -1.41$\pm$0.15, -1.44$\pm$0.24 respectively and 1.53$\pm$0.12 for the overall mean distribution. The slope of the ALTIBERG iceberg distribution is -1.52$\pm$0.07. These values are all close to the -3/2 slope already presented by (Tournadre et al., 2016) for icebergs from 0.1 to 10000 km2. A -3/2 slope has been shown both experimentally and theoretically to be representative of brittle fragmentation (Astrom, 2006; Spahn et al., 2014).

This size distribution represents a statistical view of the fragmentation process over a period of time that can correspond to several days or weeks. Indeed, it is impossible to determine from satellite image analysis or altimeter detection the exact calving time of each fragment and it is thus impossible to estimate the exact distribution of the calved pieces at their time of calving. In the same way as fragmentation is characterised by a probability distribution, the size of the fragment will also

be characterised by a probability distribution. The size distribution represents the integration over a period of time of this probability distribution. It can be used to model the transfer of volume calved from the large iceberg to small pieces.

The transfer of volume from the large icebergs to smaller pieces can also be estimated using the small iceberg area data from the ALTIBERG database. The sum of the detected pieces areas is presented in figure 11-b and d as well as the large iceberg surface loss by fragmentation. The difference between the two curves can result from, 1) an underestimation of the number of small icebergs, 2) the total area of pieces larger than ~8 km^2 not detected by altimeters. While 1 is difficult to estimate 2 can be computed, assuming that the pieces distribution follows a power law. Annex B presents the detail of the computation. For both icebergs, as long as the surface loss is limited, the number of calved pieces is small and the probability for a fragment to be too large to be detected by altimeter is also small. The total surface of the detected small icebergs represents thus almost all the parent iceberg surface loss. As the degradation increases so does the surface loss. The number of calved pieces as well as the probability of larger pieces calving become significantly larger resulting in a larger proportion of the surface loss due to pieces larger than 8 km^2 (thus not detected). The overall proportion of the surface loss due to small icebergs is about 50 % in good agreement with the power law model of Annex B.

6 Summary and conclusions

The evolution of the dimensions and shape of two large Antarctic icebergs was estimated by analysing MODIS visible images and altimeter measurements. These two giant icebergs, named B17a and C19a, were worthy of interest because they have drifted in open ocean for more than a year, relatively remote from other big icebergs, and were frequently sampled by our sensors (altimeters and MODIS). Furthermore, the two of them exhibited very different features, whether in terms of size and shape but also in their drift characteristics. We thus expect their joint studies to be an opportunity to get a more comprehensive insight into the two main processes involved in the decay of icebergs, melting and fragmentation.

Basal melting is the main cause of an iceberg's thickness decrease. We first undertook to test/prove the validity of the two main melting laws used in most numerical modelling studies by monitoring the evolution of the iceberg's thickness. We have thus computed an estimated thickness evolution according to each modelling strategy and confronted it to our measurements. The two melting models differ in their formulation since the first one is more dynamic based and the other one results from a thermodynamic balance, but both depend primarily on the same two quantities : the iceberg/water differential velocity and their temperature difference. The two modelling strategies succeed in reproducing the thickness variations of both icebergs with a high accuracy, but where the first one requires very high and unrealistic current velocities or iceberg temperatures, the second formulation fitting parameters remain within reasonable limits. If realistic current speeds and ice temperatures were to be used as inputs of the first model, it would largely underestimate the icebergs' thickness decrease, so that the second model seems more appropriate to reproduce actual melting rates. Moreover, the appropriate turbulent exchange parameters fitting the second model are found to be much smaller than used in a previous global modelling study that consequently might have overestimated the yearly freshwater flux constrained by large icebergs.

Although the main decay process of icebergs, fragmentation involves complex mechanisms and is still poorly documented. Due to the stochastic nature of fragmentation, an individual calving event can't be forecast. Yet, fragmentation can still be studied in terms of a probability distribution of a calving. We chose to carry out a sensitivity study to find out which environmental parameters are more likely to favour fracturing. We thus analysed the correlation between the relative volume loss of an iceberg and some environmental parameters. The highest correlations are found firstly for the ocean temperature and secondly for the iceberg velocity, for both B17a and C19a. All other parameters (namely the waves-related quantities) show no significant link with the volume loss. We then formulated two bulk volume loss models : firstly one that depends only on ocean temperature, and secondly one that takes into account the influence of both identified key parameters. The two formulations are fitted to our relative volume loss measurements and the best fitting parameters are estimated. Using iceberg velocity along with ocean temperature clearly better reproduces the volume loss variations, especially the quicker ones seen near the final decays of both bergs. Moreover, if the variability of the iceberg temperature is taken into account, the model coefficients are in this case quite similar for the two icebergs.

Finally, we have estimated the size distribution of the fragments calved from B17a and C19a, using MODIS images and altimetry data. For both icebergs and both methods, the slope of the distribution is close to -3/2, consistent from our previous altimetry-based global study and typical of brittle fragmentation processes.

While giant icebergs are not included in the current generation of iceberg models, they transport most of the ice volume in the Southern Ocean. Furthermore, the impact of icebergs on the ocean in global circulation models strongly depends on their size distribution. As a consequence, it is believed that the current modelling strategies suffer from a "small icebergs bias". To include them in models, we need to make sure that our previous modelling strategies are still suited to large icebergs. We also ought to gain more knowledge on how these bigger bergs constrain a size transfer to produce medium to small pieces via fragmentation. Eventually, these smaller pieces are those that account for the effective fresh water flux in the ocean. On the one hand, our study has shown that a classical modelling strategy is able to reproduce the basal melting of large icebergs, provided that relevant parameters are chosen. On the other hand, it has demonstrated that a simple bulk model with appropriate environmental parameters can be used to account for the effect of the fragmentation of large icebergs, and highlighted the consequent size distribution of the pieces. These results could prove valuable to include a more realistic representation of large icebergs in models. Our analyses could be extended to the cases of more large icebergs, namely to validate our bulk modelling approaches on a more global scale.

Acknowledgements. The MODIS images were provided by NASA through the LAADS DAAC (http://ladsweb.nascom.nasa.gov/). The altimeter data were provided by the french Centre National d'Etude Spatiale (CNES), the European Space Agency (ESA), EUMETSAT, the US National Aeronautics and Space Administration (NASA), the US National Oceanic and Atmospheric Administration and the Chinese National Ocean Satellite Application Center (NSOAS). The geostrophic current were provided by the AVISAO center (https://www.aviso.altimetry.fr). The study was partially founded by CNES through the TOSCA program.

References

Amundson, J. M. and Truffer, M.: A unifying framework for iceberg-calving models, Journal of Glaciology, 56, 822–830, doi:doi:10.3189/002214310794457173, http://www.ingentaconnect.com/content/igsoc/jog/2010/00000056/00000199/art00008, 2010.

Arthern, R., Vaughan, D., Rankin, A., Mulvaney, R., and Thomas, E. R.: In situ measurements of Antarctic snow compaction compared with predictions of models, J. Geophys. Res., 115, doi:10.1029/2009JF001306, 2010.

Astrom, J. A.: Statistical models of brittle fragmentation, Advances in Physics, 55, 247–278, doi:10.1080/00018730600731907, http://dx.doi.org/10.1080/00018730600731907, 2006.

Bassis, J.: The statistical physics of iceberg calving and the emergence of universal calving laws, Journal of Glaciology, 57, 3–16, doi:doi:10.3189/002214311795306745, http://www.ingentaconnect.com/content/igsoc/jog/2011/00000057/00000201/art00001, 2011.

Benn, D., C.R., W., and R.H., M.: Calving processes and the dynamics of calving glaciers, Earth Sci. Rev., 82, 143–179, 2007.

Bigg, G., Wadley, M., Stevens, D., and Johnson, J.: Modelling the dynamics and thermodynamics of icebergs, Cold Regions Scienc. Techn., 26(2), 113–135, doi:10.1016/S0165-232X(97)00012-8, 1997.

Diemand, D.: Icebergs, in: Encyclopedia of Ocean Sciences, edited by Steele, J. H., pp. 1255–1264, Academic Press, Oxford, doi:10.1006/rwos.2001.0002, http://www.sciencedirect.com/science/article/B77C6-4B0FVKG-2/2/93bf19ca1170a3102602c927c99bfb01, 2001.

Fricker, H. A., Young, N. W., Allison, I., and Coleman, R.: Iceberg calving from the Amery Ice Shelf, East Antarctica, Annals of Glaciology, 34, 241–246, doi:10.3189/172756402781817581, 2002.

Gladstone, R. M., Bigg, G. R., and Nicholls, K. W.: Iceberg trajectory modeling and meltwater injection in the Southern Ocean, J. Geophys. Res., 106, 19 903–19 916, doi:10.1029/2000JC000347, 2001.

Goodman, D. J., Wadhams, P., and Squire, V. A.: The flexural response of a tabular ice island to ocean swell, Annals of Glaciology, 1, 23–27, 1980.

Hamley, T. C. and Budd, W. F.: Antarctic iceberg distribution and dissolution, J. Glaciol., 32, 242–251, 1986.

Hellmer, H. H. and Olbers, D.: A two-dimensional model for the thermohaline circulation under an ice shelf., Antarctic Science, 3, 433–442, 1989.

Helly, J. J., Kaufmann, R. S., Stephenson Jr., G. R., and Vernet, M.: Cooling, dilution and mixing of ocean water by free-drifting icebergs in the Weddell Sea, Deep Sea Res. Part II: Topical Studies in Oceanography, 58, 1346–1363, doi:10.1016/j.dsr2.2010.11.010, http://www.sciencedirect.com/science/article/pii/S0967064510003668, 2011.

Holdsworth, G. and Glynn, J.: Iceberg calving from floating glaciers by a vibrating mechanism,, Nature, 274, 464–466., 1978.

Holland, D. M. and Jenkins, A.: Modeling Thermodynamic Ice–Ocean Interactions at the Base of an Ice Shelf, Journal of Physical Oceanography, 29, 1787–1800, doi:10.1175/1520-0485(1999)029<1787:MTIOIA>2.0.CO;2, http://dx.doi.org/10.1175/1520-0485(1999)029<1787:MTIOIA>2.0.CO;2, 1999.

Huppert, H. E. and Josberger, E. G.: The Melting of Ice in Cold Stratified Water, Journal of Physical Oceanography, 10, 953–960, doi:10.1175/1520-0485(1980)010<0953:TMOIIC>2.0.CO;2, http://dx.doi.org/10.1175/1520-0485(1980)010<0953:TMOIIC>2.0.CO;2, 1980.

Jacka, T. H. and Giles, A. B.: Antarctic iceberg distribution and dissolution from ship-based observations, J. Glaciol., 53, 341–356, 2007.

Jansen, D., Sandhäger, H., and Rack, W.: Model experiments on large tabular iceberg evolution: ablation and strain thinning, Journal of Glaciology, 51, 363–372, doi:doi:10.3189/172756505781829313, http://www.ingentaconnect.com/content/igsoc/jog/2005/00000051/00000174/art00003, 2005.

Jansen, D., Schodlok, M., and Rack, W.: Basal melting of A-38B: A physical model constrained by satellite observations, Rem. Sens. Environ., 111, 195–203, doi:10.1016/j.rse.2007.03.022, http://www.sciencedirect.com/science/article/pii/S0034425707002878, Remote Sensing of the Cryosphere Special Issue, 2007.

Jongma, J. I., Driesschaert, E., Fichefet, T., Goosse, H., and Renssen, H.: The effect of dynamic-thermodynamic icebergs on the Southern Ocean climate in a three-dimensional model, Ocean Modelling, 26, 104–113, doi:DOI: 10.1016/j.ocemod.2008.09.007, http://www.sciencedirect.com/science/article/B6VPS-4TN0M2H-1/2/9303a7a08d2263a3b37b3ec60e35dfe6, 2009.

Kader, B. A. and Yaglom, A. M.: Heat and mass transfer laws for fully turbulent wall flows, Int. J. Heat Mass Transfer, 15, 2329–2351, 1972.

Li, J. and Zwally, H.: Modeling of firn compaction for estimating ice-sheet mass change from observed ice-sheet elevation change, Annal. Glacio., 52(59), 1–7, 2011.

Ligtenberg, S. R. M., Helsen, M. M., and van den Broeke, M. R.: An improved semi-empirical model for the densification of Antarctic firn, The Cryosphere, 5, 809–819, doi:10.5194/tc-5-809-2011, http://www.the-cryosphere.net/5/809/2011/, 2011.

Løset, S.: Thermal energy conservation in icebergs and tracking by temperature, Journal of Geophysical Research: Oceans, 98, 10 001–10 012, doi:10.1029/93JC00138, http://dx.doi.org/10.1029/93JC00138, 1993.

MacAyeal, D. R., Okal, E. A., Aster, R. C., Bassis, J. N., Brunt, K. M., Cathles, L. M., Drucker, R., Fricker, H. A., Kim, Y.-J., Martin, S., Okal, M. H., Sergienko, O. V., Sponsler, M. P., and Thom, J. E.: Transoceanic wave propagation links iceberg calving margins of Antarctica with storms in tropics and Northern Hemisphere, Geophysical Research Letters, 33, n/a–n/a, doi:10.1029/2006GL027235, http://dx.doi.org/10.1029/2006GL027235, l17502, 2006.

Marsh, R., Ivchenko, V. O., Skliris, N., Alderson, S., Bigg, G. R., Madec, G., Blaker, A. T., Aksenov, Y., Sinha, B., Coward, A. C., Le Sommer, J., Merino, N., and Zalesny, V. B.: NEMO–ICB (v1.0): interactive icebergs in the NEMO ocean model globally configured at eddy-permitting resolution, Geoscientific Model Development, 8, 1547–1562, doi:10.5194/gmd-8-1547-2015, http://www.geosci-model-dev.net/8/1547/2015/, 2015.

Martin, T. and Adcroft, A.: Parameterizing the fresh-water flux from land ice to ocean with interactive icebergs in a coupled climate model, Ocean Modelling, 34, 111–124, doi:10.1016/j.ocemod.2010.05.001, 2010.

McIntyre, N. F. and Cudlip, W.: Observation of a giant Antarctic tabular iceberg by satellite radar altimetry, Polar Rec., 145, 458–462, 1987.

Merino, N., Sommer, J. L., Durand, G., Jourdain, N. C., Madec, G., Mathiot, P., and Tournadre, J.: Antarctic icebergs melt over the Southern Ocean : Climatology and impact on sea ice, Ocean Modelling, 104, 99–110, doi:10.1016/j.ocemod.2016.05.001, http://www.sciencedirect.com/science/article/pii/S1463500316300300, 2016.

Neshyba, Steve, E. G. J.: On the estimation of Antarctic iceberg melt rate, J. Phys. Oceanogr., 10, 1681–1685, 1980.

Reeh, N.: A nonsteady-state firn-densification model for the percolation zone of a glacier, Journal of Geophysical Research: Earth Surface, 113, n/a–n/a, doi:10.1029/2007JF000746, http://dx.doi.org/10.1029/2007JF000746, f03023, 2008.

Savage, S.: Aspects of Iceberg Deterioration and Drift, pp. 279–318, Springer Berlin Heidelberg, Berlin, Heidelberg, doi:10.1007/3-540-45670-8_12, http://dx.doi.org/10.1007/3-540-45670-8_12, 2001.

Savage, S., Crocker, G., Sayed, M., and Carrieres, T.: Size distributions of small ice pieces calved from icebergs, Cold Regions Science and Technology, 31, 163 – 172, doi:https://doi.org/10.1016/S0165-232X(00)00010-0, http://www.sciencedirect.com/science/article/pii/S0165232X00000100, 2000.

Scambos, T., Sergienko, O., Sargent, A., McAyeal, D., and Fastbook, J.: ICESat profiles of tabular iceberg margins and iceberg breakup at low latitudes, Geophys. Res. Let., 32, doi:10.1029/2005GL023802, 2005.

Scambos, T., Ross, R., Bauer, R., Yermolin, Y., Skvarca, P., Long, D., Bohlander, J., and Haran, T.: Calving and ice-shelf break-up processes investigated by proxy: Antarctic tabular iceberg evolution during northward drift, J. Glaciol., 54, 579–591, doi:10.3189/002214308786570836, http://www.ingentaconnect.com/content/igsoc/jog/2008/00000054/00000187/art00002, 2008.

Schodlok, M. P., Hellmer, H. H., Rohardt, G., and Fahrbach, E.: Weddell Sea iceberg drift: Five years of observations, J. Geophys. Res., 111, C06 018, doi:10.1029/2004JC002661., 2006.

Schwerdtfeger, P.: Iceberg oscillations and ocean waves, An. Glaciol., 1, 63–65, 1980.

Silva, T., Bigg, G., and Nicholls, K.: The contribution of giant icebergs to the Southern Ocean freshwater flux, J. Geophys. Res., 111, C03 004, doi:10.1029/2004JC002843, 2006.

Spahn, F., Neto, E. V., Guimarães, A. H. F., Gorban, A. N., and Brilliantov, N. V.: A statistical model of aggregate fragmentation, New Journal of Physics, 16, 013 031, http://stacks.iop.org/1367-2630/16/i=1/a=013031, 2014.

Stern, A. A., Adcroft, A., and Sergienko, O.: The effects of Antarctic iceberg calving-size distribution in a global climate model, Journal of Geophysical Research: Oceans, 121, 5773–5788, doi:10.1002/2016JC011835, 2016.

Stuart, K. M. and Long, D. G.: Tracking large tabular icebergs using the SeaWinds Ku-band microwave scatterometer, Deep Sea Res. Part II-Topical studies in Oceanography., 58, 1285–1300, doi:10.1016/j.dsr2.2010.11.004, 2011.

Tournadre, J.: Signature of Lighthouses, Ships, and Small Islands in Altimeter Waveforms, J. Atmos. Oceanic Tech., 24, 1143–1149, 2007.

Tournadre, J., Bouhier, N., Girard-Ardhuin, F., and Rémy, F.: Large icebergs characteristics from altimeter waveforms analysis, J. Geophys. Res., 120, 1954–1974, doi:10.1002/2014JC010502, 2015.

Tournadre, J., Bouhier, N., Girard-Ardhuin, F., and Remy, F.: Antarctic icebergs distributions 1992-2014, J. Geophys. Res., 121, 327–349, doi:10.1002/2015JC011178, 2016.

Venkatesh, S.: On the Deterioration of a Grounded Iceberg, Journal of Glaciology, 32, 161–167, doi:10.1017/S0022143000015471, 1986.

Wadhams, P., Kristensen, M., and Orheim, O.: The response of Antarctic icebergs to ocean waves, Journal of Geophysical Research: Oceans, 88, 6053–6065, doi:10.1029/JC088iC10p06053, http://dx.doi.org/10.1029/JC088iC10p06053, 1983.

Wagner, T. J. W., Wadhams, P., Bates, R., Elosegui, P., Stern, A., Vella, D., Abrahamsen, E. P., Crawford, A., and Nicholls, K. W.: The "footloose" mechanism: Iceberg decay from hydrostatic stresses, Geophys. Res. Let., 41, 5522–5529, doi:10.1002/2014GL060832, http://dx.doi.org/10.1002/2014GL060832, 2014.

Wagner, T. J. W., Dell, R. W., and Eisenman, I.: An Analytical Model of Iceberg Drift, Journal of Physical Oceanography, 47, 1605–1616, doi:10.1175/JPO-D-16-0262.1, https://doi.org/10.1175/JPO-D-16-0262.1, 2017.

Weeks, W. F. and Campbell, W. J.: Icebergs as a Fresh-Water Source: An Appraisal, Journal of Glaciology, 12, 207–233, 1973.

West, J. C. and Demarest, R.: The radiation characteristics of an arbitary antenna positioned on a polar ice sheet,, Geophys., 12, 1689–1696, 1987.

Appendix A: Firn densification

The process of firn densification is complex and although several models have been developed for ice sheet (Reeh, 2008; Arthern et al., 2010; Li and Zwally, 2011; Ligtenberg et al., 2011), at present, no reliable model exists for icebergs who

The Cryosphere Discuss., https://doi.org/10.5194/tc-2017-208
Manuscript under review for journal The Cryosphere
Discussion started: 14 November 2017

experienced more variable oceanic and atmospheric conditions. However, the change of free-board induced by firn densification can be estimated using a simple model. Icebergs density profile can be represented by an exponential profile in the form

$$\rho(\mathrm{z}) = \rho_i - Ve^{R\mathrm{z}}$$

where z is the depth, ρ the density and ρ_i the density of pure ice (915 kg.m^3) (West and Demarest, 1987). The V and R model parameters are tuned so that the depths of the 550 and 830 kg.m^3 densities correspond to the mean values of the firn column on big ice shelves presented by Ligtenberg et al. (2011), i.e. 5 and 45 m respectively. The change of free-board induced by firn densification is estimated by simple integration of the density profile and by assuming that all the firn layer densifies in the same proportion. Figure A1 presents the change of thickness and free-board and thickness for a 450 m thick iceberg as a function of the proportion of densification. The decrease of thickness and free-board is below 4 m and 1 m for a 25% and 6.1 m and 2.1 m for a 50% one. These values exceed, although significant, are small compared to the change of thickness and free-board measured during the two icebergs drift that are of the order of 100-200 m and 20-30 m respectively. However, the firn densification will lead to an overestimation of the iceberg melt rate that could be of the order of 2-5%.

Appendix B: Power law and total area distribution

The fragment size probability follows a power law with a -3/2 slope for sizes between s_1 and s_2 thus

$$P(s) = \alpha_0 s^{-3/2} \tag{B1}$$

where $\alpha_0 = \sqrt{s_0 s_1}/(2(\sqrt{s_1} - \sqrt{s_0}))$.

If $N_0$is the number of calved icebergs of sizes between s_3 and s_4, then the distribution of the number N is $N(s) = N_0\alpha_0 s^{-3/2}$. The maximum iceberg size s_{lim}, i.e. the class for which $N(s_{lim}) = 1$ is $s_{lim} = (N_0\alpha_0)^{2/3}$. The proportion of the total surface represented by the icebergs of sizes between s_3 and s_4 is thus

$$R(N_0) = \frac{\int_{s_3}^{s_4} N_0\alpha_0 s\, s^{3/2} ds}{\int_{s_1}^{s_{lim}} N_0\alpha_0 s\, s^{3/2} ds} = \frac{\sqrt{s_4} - \sqrt{s_3}}{\sqrt{(N_0\alpha_0)^{2/3}} - \sqrt{s_1}} \tag{B2}$$

Figure B1 presents R for s_4 from 4 to 9 km^2, $s_1 = 0.01$km^2, i.e. the smallest iceberg detectable using MODIS, $s_3 = 0.1$km^2, i.e. the detection limit of altimeter, s_2 has been set to 40 km^2, size of the largest piece detected on the MODIS images. If a thousand fragments have been created, icebergs smaller than 6 km^2 represents only 60% of the total surface, the ones smaller than 8 km^2 70%. For 2000 fragments, the proportion drops to 50 and 55% respectively.

Competing interests. None

The Cryosphere Discuss., https://doi.org/10.5194/tc-2017-208
Manuscript under review for journal The Cryosphere
Discussion started: 14 November 2017

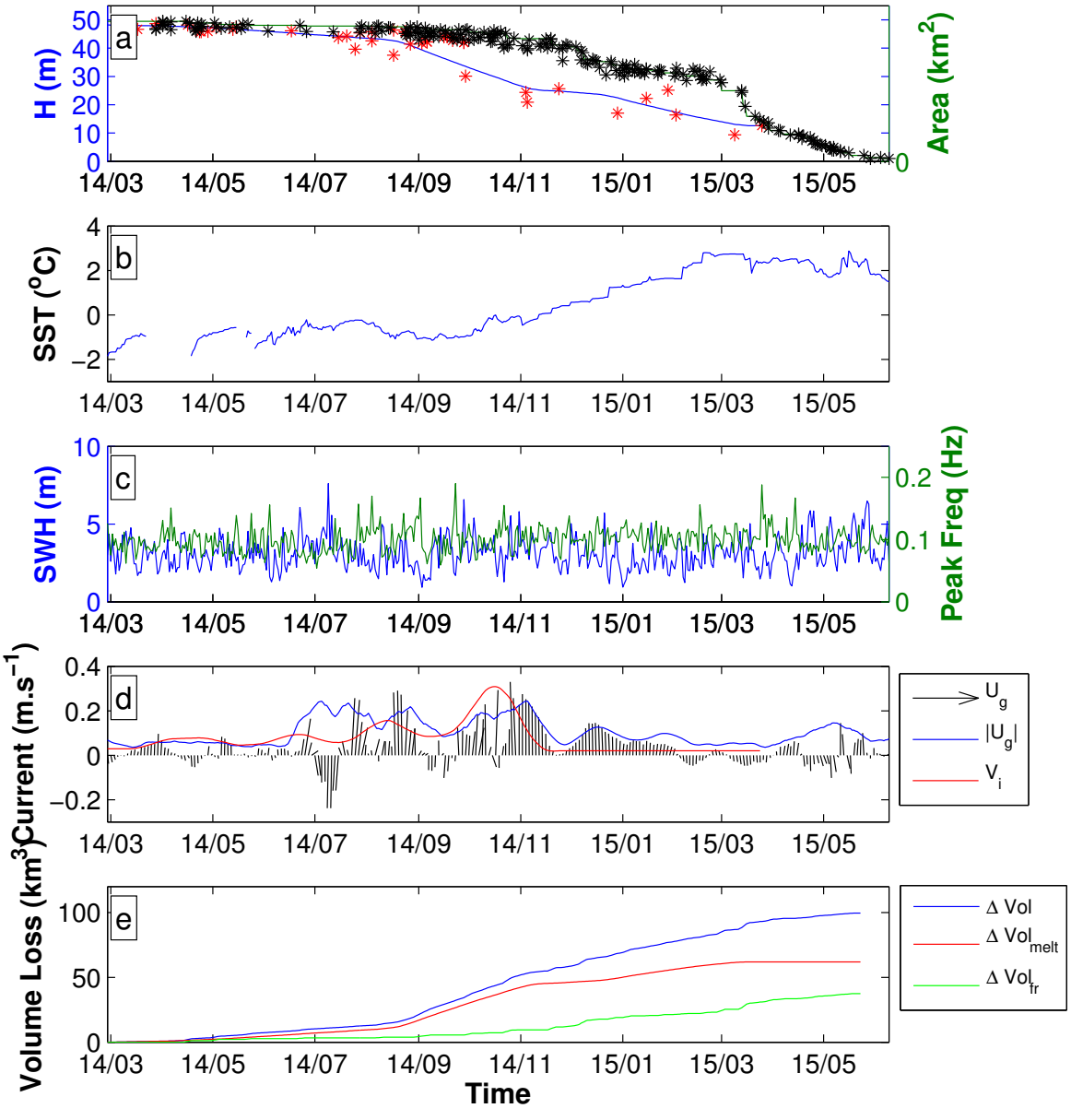

Figure 4. (a) B17a Area (in km^2) and free-board (in m). The green and blue line represent the interpolated daily area and free-board and the black and red crosses the MODIS area and altimeter free-board estimates. (b) ODYSSEA Sea surface temperature (in °C). (c) Significant wave height in m (blue line) and peak frequency in Hz (green line). (d) AVISO geostrophic current (black arrows) and current velocity (blue line) and iceberg velocity (red line) . (e) Total volume loss (blue line), volume loss by melting (red line) and by fragmentation (green line).

The Cryosphere Discuss., https://doi.org/10.5194/tc-2017-208
Manuscript under review for journal The Cryosphere
Discussion started: 14 November 2017

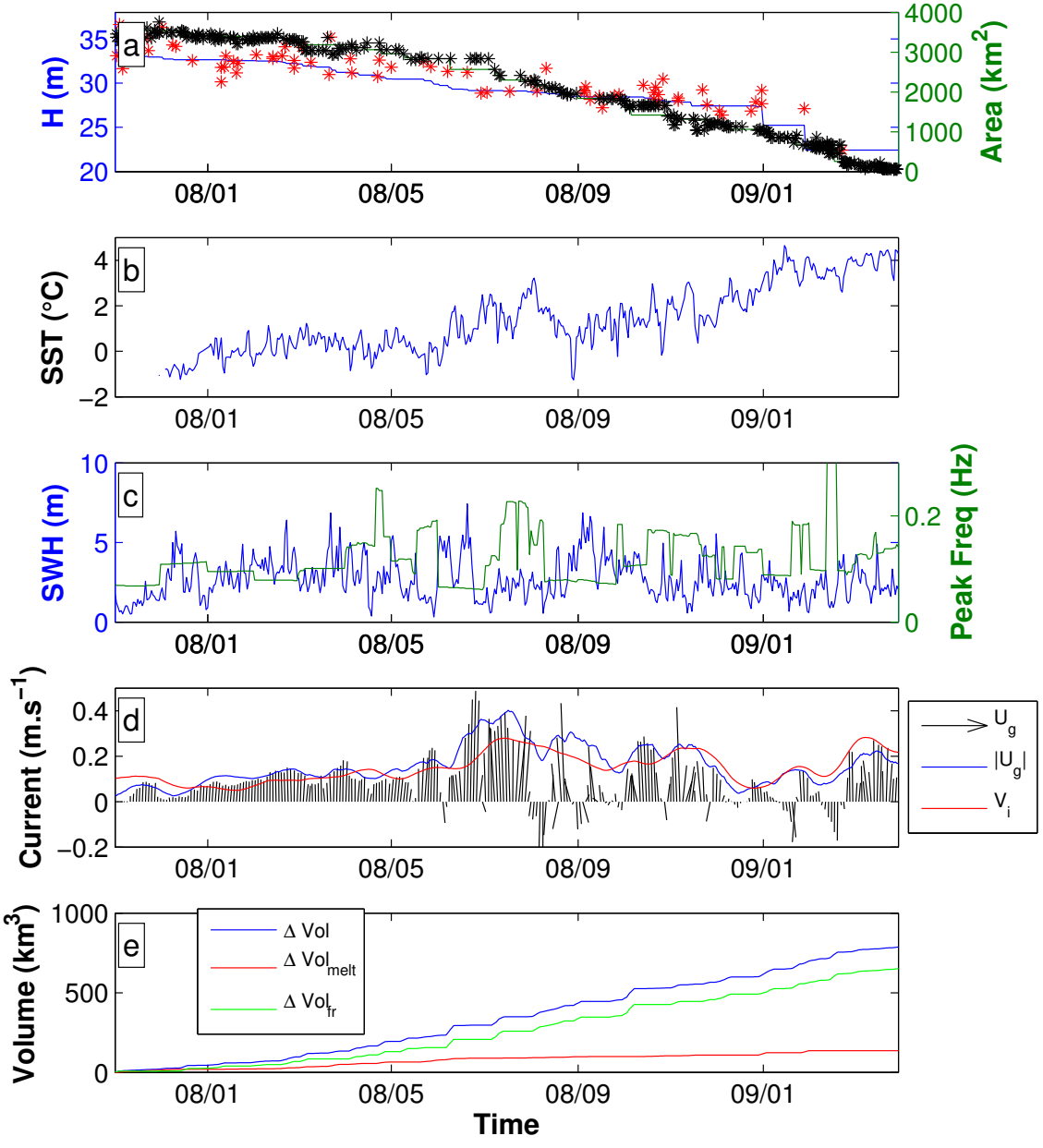

Figure 5. (a) C19a Area (in km^2) and free-board (in m). The green and blue line represent the interpolated daily area and free-board and the black and red crosses the MODIS area and altimeter free-board estimates. (b) ODYSSEA Sea surface temperature (in °C). (c) Significant wave height in m (blue line) and peak frequency in Hz (green line). (d) AVISO geostrophic current (black arrows) and current velocity (blue line) and iceberg velocity (red line). (e) Total volume loss (blue line), volume loss by melting (red line) and by fragmentation (green line). .

The Cryosphere Discuss., https://doi.org/10.5194/tc-2017-208
Manuscript under review for journal The Cryosphere
Discussion started: 14 November 2017

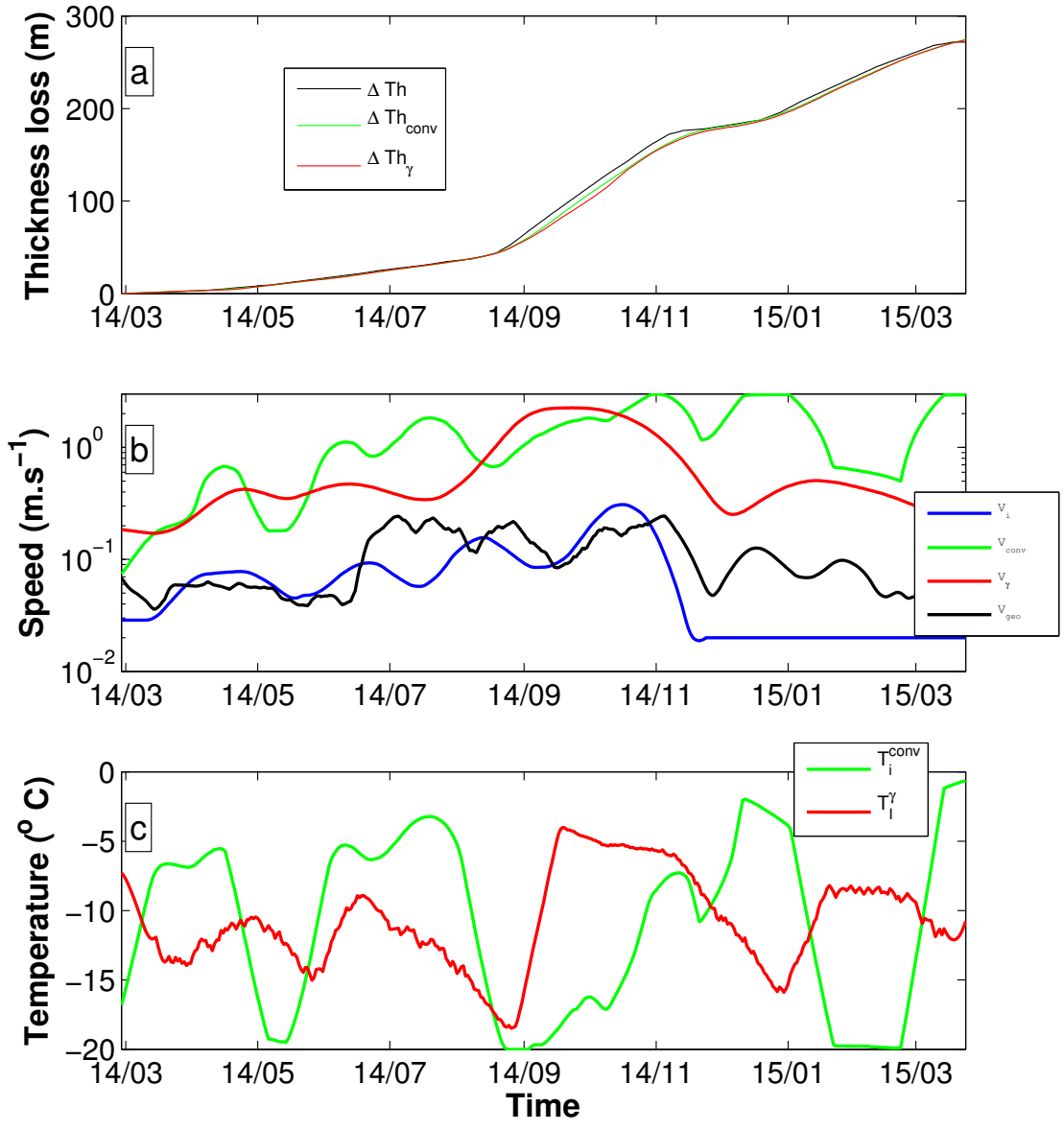

Figure 6. Thickness loss (in m) for B17a (a). Measured thickness loss (blue line); modelled loss using forced convection (green line) and turbulent exchange (red line). (b) Iceberg velocity (blue line). Modelled velocity using forced convection (red line) and using turbulent exchange (green line). AVISO Geostrophic current velocity (black) line. (c) Modelled iceberg temperature using forced convection (blue line) and using thermal exchange (green line).

The Cryosphere Discuss., https://doi.org/10.5194/tc-2017-208
Manuscript under review for journal The Cryosphere
Discussion started: 14 November 2017

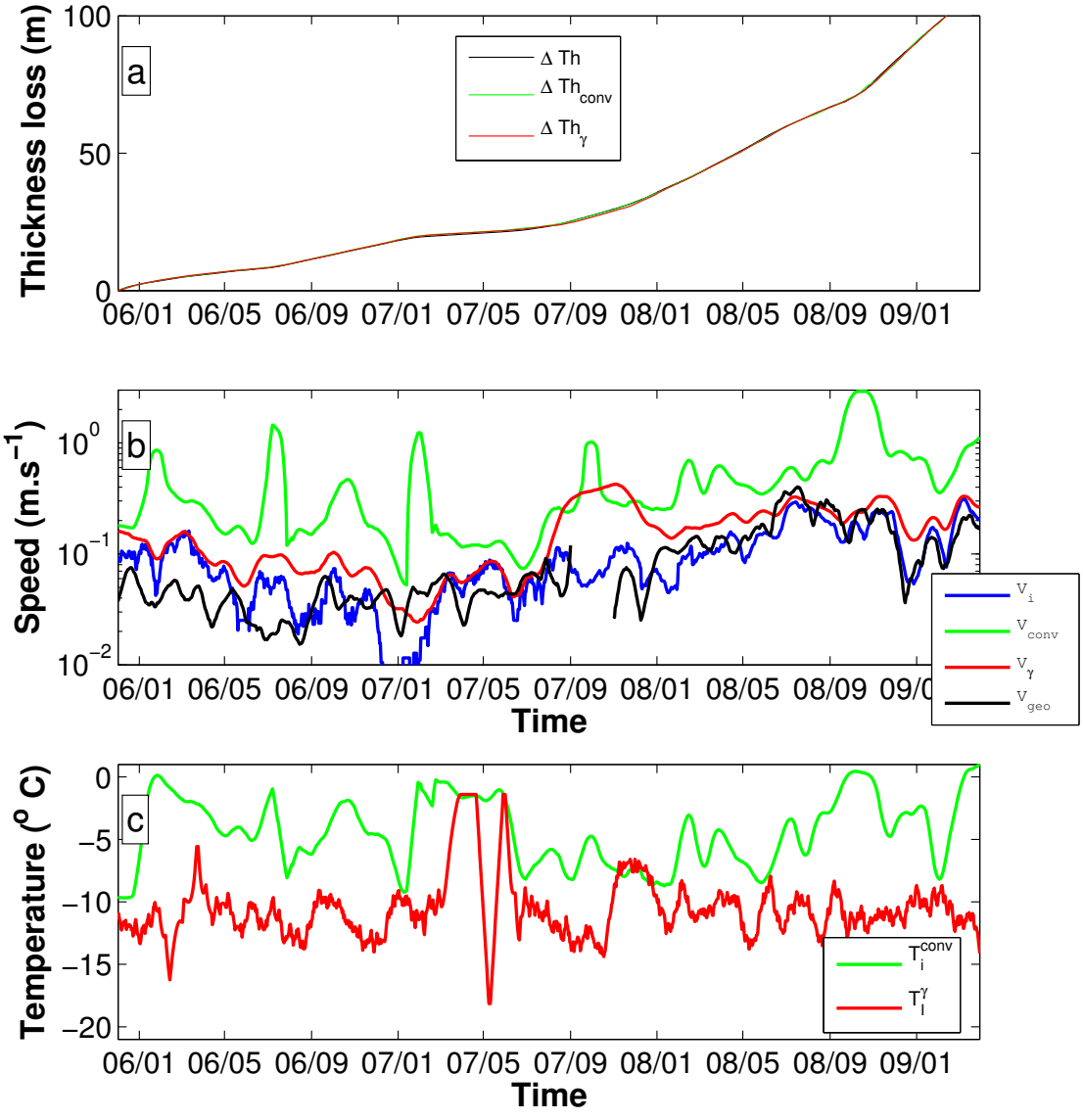

Figure 7. Thickness loss (in m) for C19a (a). Measured thickness loss (blue line); modelled loss using forced convection (green line) and turbulent exchange (red line). (b) Iceberg velocity (blue line). Modelled velocity using forced convection (red line) and using turbulent exchange (green line). AVISO Geostrophic current velocity (black) line. (c) Modelled iceberg temperature using forced convection (blue line) and using thermal exchange (green line).

The Cryosphere Discuss., https://doi.org/10.5194/tc-2017-208
Manuscript under review for journal The Cryosphere
Discussion started: 14 November 2017

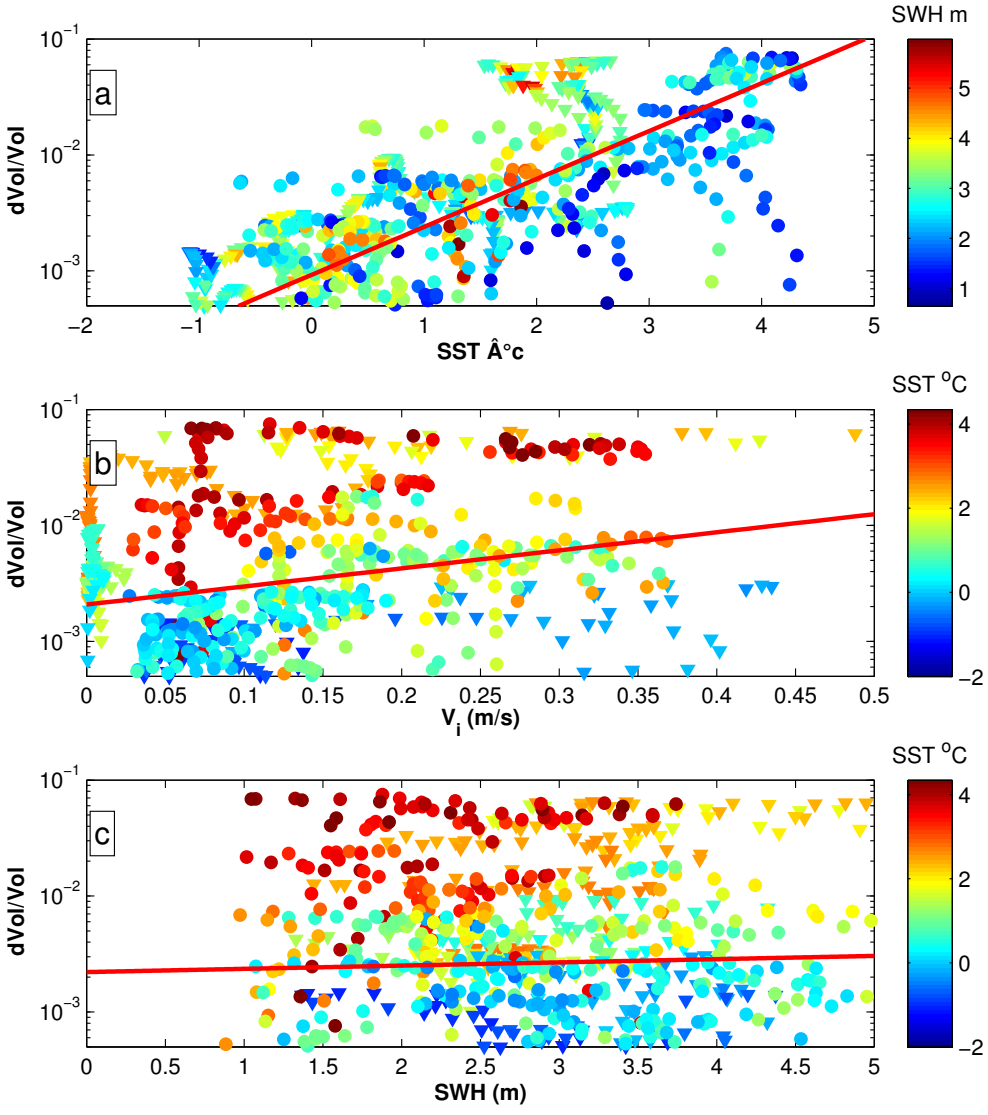

Figure 8. (a) Relative volume loss dV/V as a function of SST. The colour represents the significant wave height in m. (b) dV/V as a function of the iceberg velocity. The colour represents the SST in °C. (c) dV/V as a function of significant wave height. The circles correspond to C19a and the triangle to B17a. The red lines represent the regression lines.. The ordinate scale is logarithmic.

The Cryosphere Discuss., https://doi.org/10.5194/tc-2017-208
Manuscript under review for journal The Cryosphere
Discussion started: 14 November 2017

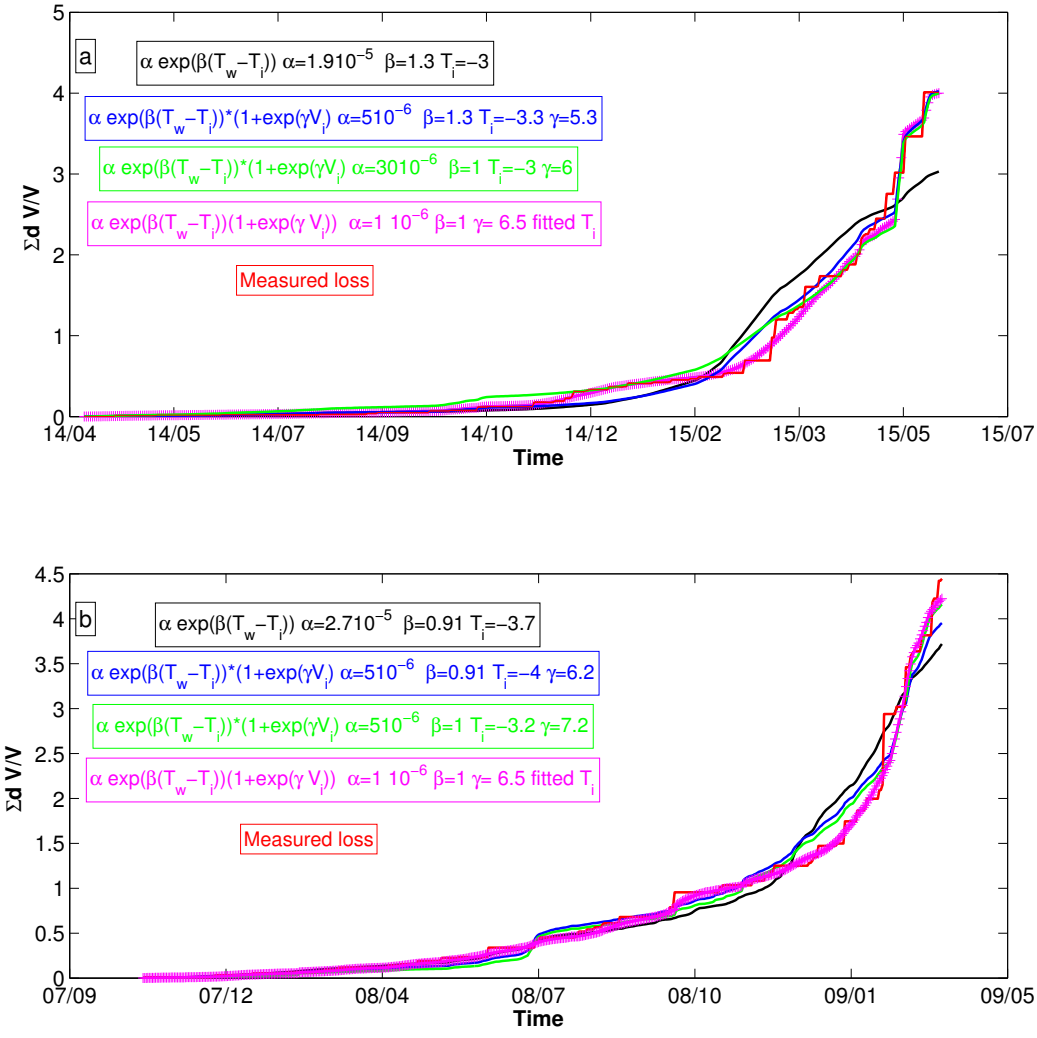

Figure 9. (a) Cumulative relative volume loss, $\sum dV/V$, measured (red line), model depending on temperature difference only (black line), on temperature difference and iceberg velocity (blue line), on temperature difference and iceberg velocity with $\beta = 1$ (green line), full model fitted piece-wise (magenta line). (a) B17a, (b) C19a.

The Cryosphere Discuss., https://doi.org/10.5194/tc-2017-208
Manuscript under review for journal The Cryosphere
Discussion started: 14 November 2017

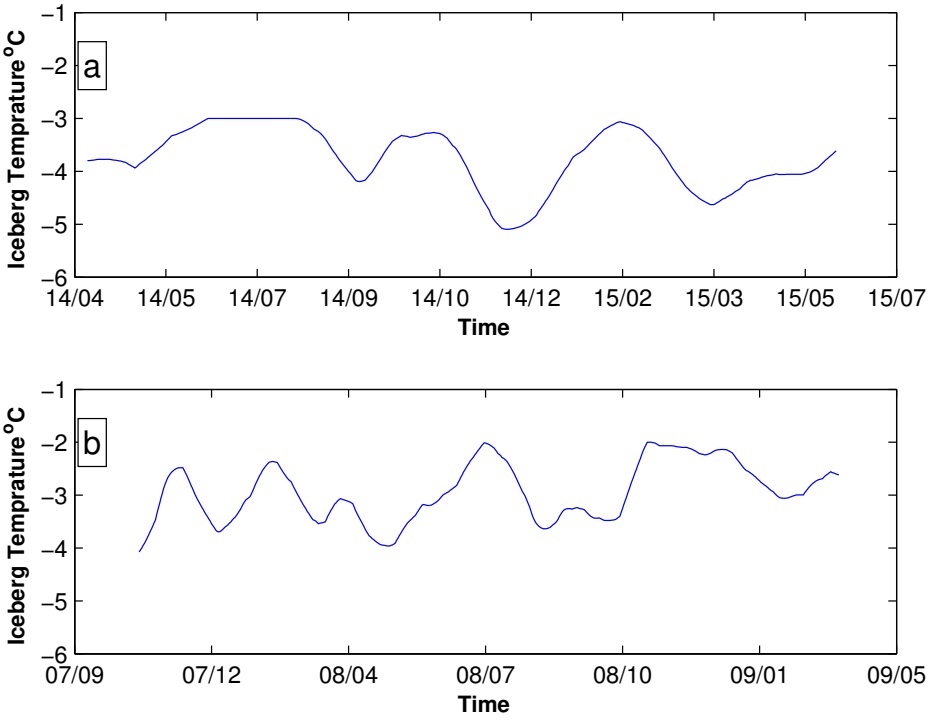

Figure 10. Fitted iceberg temperature for B17a (a) and C19a (b).

The Cryosphere Discuss., https://doi.org/10.5194/tc-2017-208
Manuscript under review for journal The Cryosphere
Discussion started: 14 November 2017

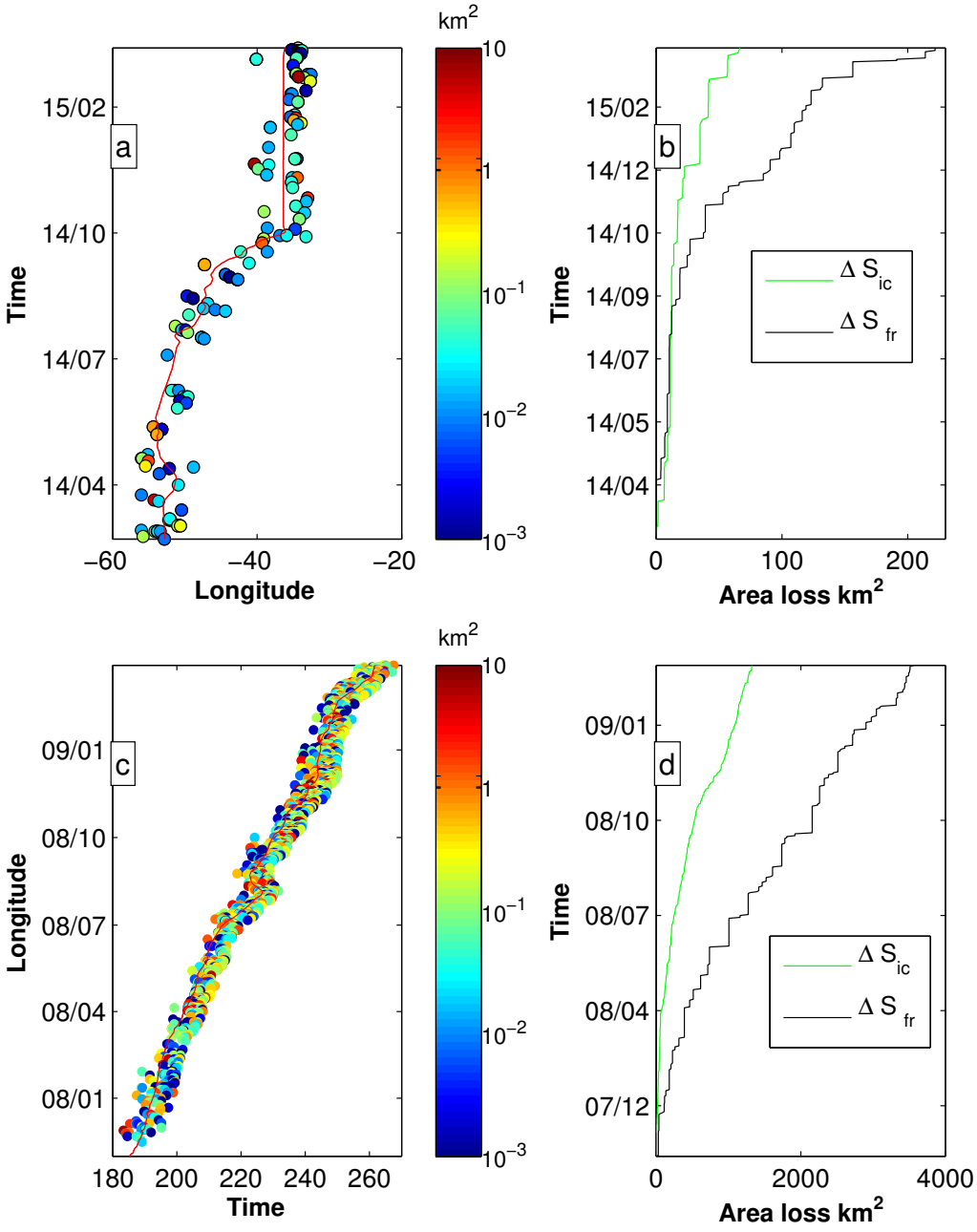

Figure 11. Time/longitude trajectory of B17a (a) and C19a (c) and coincident small icebergs detected in its vicinity. The colour represents the area of the iceberg in log scale. Surface loss by breaking (black lines) and surface of the detected small icebergs (green line) for B17a (b) and C19a (d).

The Cryosphere Discuss., https://doi.org/10.5194/tc-2017-208
Manuscript under review for journal The Cryosphere
Discussion started: 14 November 2017

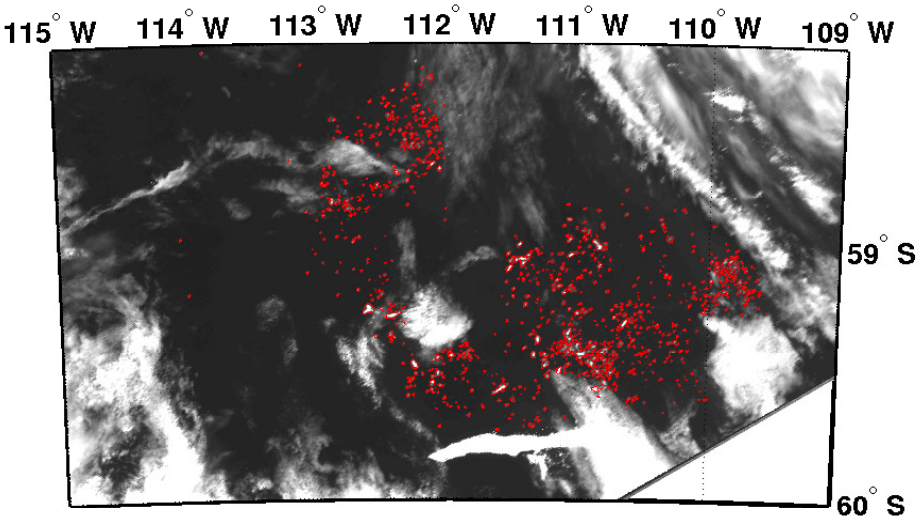

Figure 12. Example of fragment detection using a MODIS image (C19a 02/05/2009). The contour of the detected icebergs are represented in red lines.

The Cryosphere Discuss., https://doi.org/10.5194/tc-2017-208
Manuscript under review for journal The Cryosphere
Discussion started: 14 November 2017

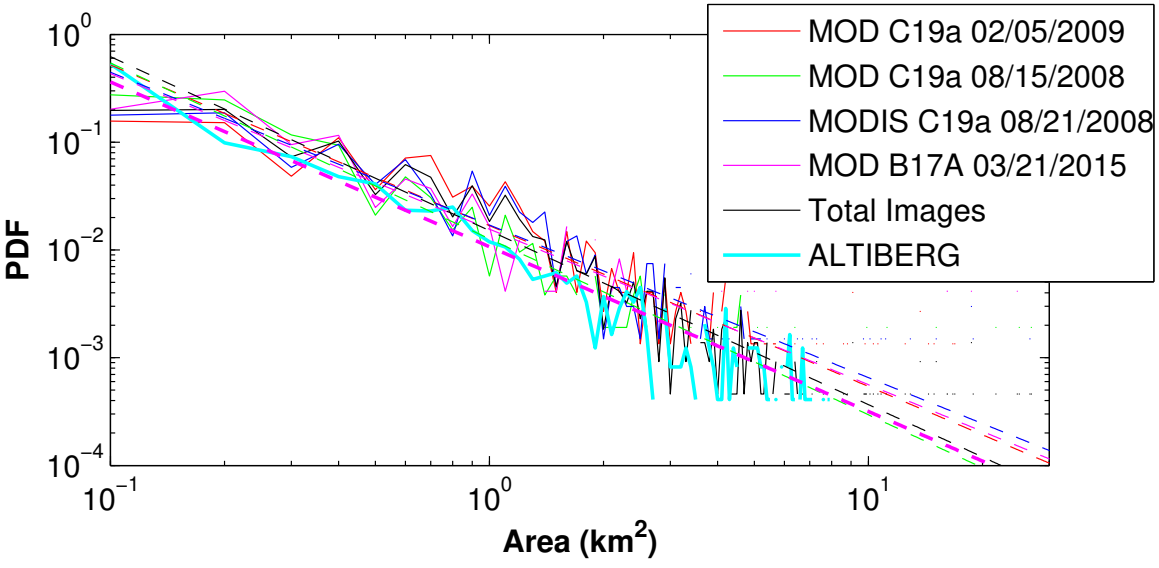

Figure 13. Probability density function of the fragment size detected on MODIS images (red line C19a 02/05/2009, green line C19a 08/15/2008, blue line 08/21/200, magenta line B17a 03/02/2015, black line all images), and detected by altimeter in the vicinity of C19a (cyan line).

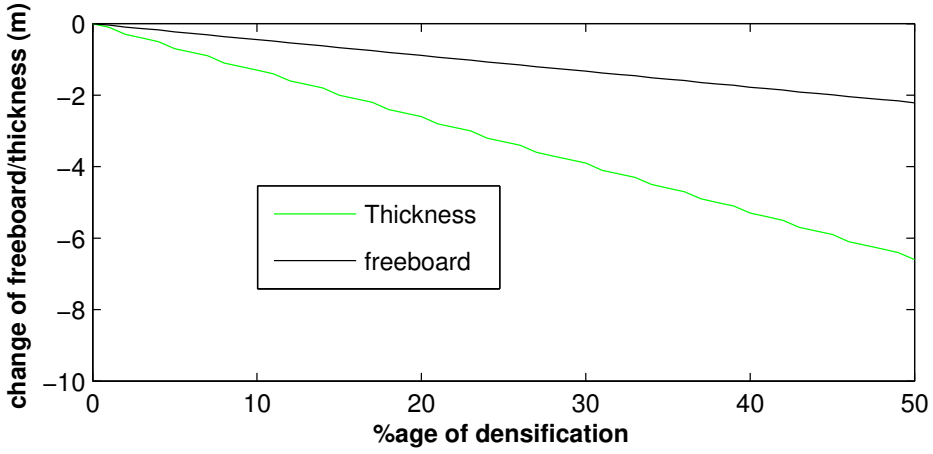

Figure A1. Variation of thickness (green line) and free-board (black line) as a function of the percentage of firn densification for a 450 m thick iceberg

The Cryosphere Discuss., https://doi.org/10.5194/tc-2017-208
Manuscript under review for journal The Cryosphere
Discussion started: 14 November 2017

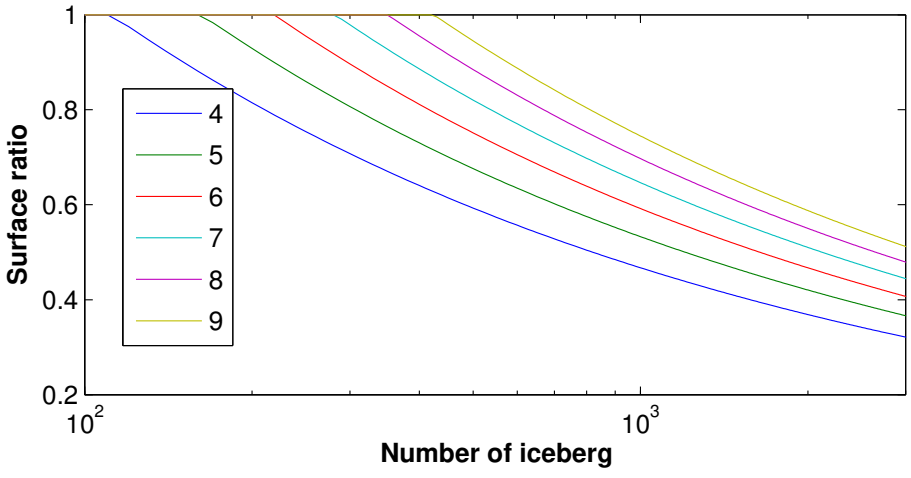

Figure B1. Proportion of the total surface represented by icebergs of area between 0.1 and 4 to 9 km^2 as a function of the total number of icebergs.